JOURNAL OF AIRCRAFT
Vol. 47, No. 3, May–June 2010

Computational-Fluid-Dynamics- and Computational-Structural-Dynamics-Based Time-Accurate Aeroelasticity of Helicopter Rotor Blades

G. P. Guruswamy*
NASA Ames Research Center, Moffett Field, California 94035

DOI: 10.2514/1.45744

A modular capability to compute dynamic aeroelastic characteristics of rotor blades using the Euler/Navier–Stokes flow equations and finite element structural equations is presented. The approach is based on a time-accurate analysis procedure that is suitable for nonlinear fluid–structure interaction problems. Fluids and structural solvers are time-accurately coupled in the C++ environment. Unsteady aerodynamic and aeroelastic results are validated with experimental data for nonrotating and rotating isolated blades.

Introduction

COMPUTATIONAL aeroelasticity is one of the most challenging fields for both rotorcraft and aircraft. Flutter "that makes or breaks a vehicle" is an aeroelastic instability caused by strong coupling of fluid and structural forces. In particular, the behavior of rotary wings is inherently flexible and dynamic, requiring time-accurate methods to compute aeroelastic characteristics.

Aerodynamic methods based on linear theory are well established for today's rotorcraft applications, resulting in advanced codes such as the rotorcraft comprehensive analysis system [1] and comprehensive analytical model of rotorcraft aerodynamics and dynamics [2]. These codes, traditionally known as comprehensive codes (CC), include structural modeling techniques based on nonlinear beam theory. In comprehensive codes, the linear aerodynamic parameters are either expressed as a function of structural parameters or specified using empirical theories. While comprehensive codes have performed well in the linear flow regime, their use is stretched beyond their realm of applicability to nonlinear flow regimes [3]. To overcome the inabilities of linear theories to compute complex flows involving moving shock waves and flow separation, methods based on the Euler/Navier–Stokes equations are essential [4]. At the same time, computational fluid dynamics (CFD) needs to be time-accurately coupled with advanced computational structural dynamics (CSD) capabilities to capture the physics related to dynamic aeroelastic effects.

Since development of the first unsteady 2-D transonic code, LTRAN2 [5], in the mid-1970s, use of CFD for aeroelasticity has made continuous impacts on both aircraft and rotorcraft. The first validated results obtained by the time-accurate coupling of finite-difference-based fluids equations with finite-element-based structures equations for blade sections using LTRAN2 are reported in [6]. LTRAN2 is the first CFD code applied to unsteady blade–vortex interaction simulations [7] of rotor blades. Reviews of rotary wing aeroelasticity are reported in survey papers [8,9]. The first fully validated procedure to compute CFD/CSD-based transonic aeroelasticity of fixed blades is presented in [10].

Finite-element-method-based CSD and finite-difference-method-based CFD have grown continuously since the mid-1950s and early 1970s, respectively. The levels of fidelity (see Fig. 1) in both areas increased along with increased availability of computer power. Time-accurately-coupled CFD/CSD methods for aircraft are adequately mature for solving full configurations [11]. Many complex configurations have been solved using NASA's advanced aeroelastic software, HiMAP [12].

In contrast to the situation for fixed-wing aircraft, the CFD/CSD-based time-accurate aeroelastic methods for rotorcraft are significantly lagging, as shown in Fig. 1. The arrows in Fig. 1 are applicable to both fluids and structures. The arrow related to complexity indicates the ease with which complex geometries can be modeled using lower-fidelity models. As reported in [13], the current validated state of the art is the quasi-steady or loosely coupled approach based on hybrid CFD and CC methods [14]. Computational structural dynamics used in the CC method are limited to simple beam models, mostly in harmonic motions. Recently, hybrid methods were extended to tightly coupled computations [15], but these have not yet been validated. Since CFD computations are coupled in an ad hoc fashion with CC computations [15], it may not be adequate to maintain time accuracy in nonlinear flow regimes in which the hybrid CFD-CC method is neither valid nor suitable for transient conditions [13]. Furthermore, the inability to predict phase angles for flapping motion may be a strong indication of inadequacies in the approach [16].

Within the Fundamental Aeronautics Program, NASA has initiated an effort to develop CFD/CSD-coupled methods from first principles, differing from current approaches in which CFD is run in a slave mode by hybriding with comprehensive codes [15]. Development will be validated using classical test cases including all possible physics-based modeling in a CFD/CSD-coupled approach. From the configuration point of view, it will be more of a bottoms-up approach rather than the current top-down approach [17], which tries to address missing physics such as flexibility after the fact. In addition, good balance in the fidelity (becoming important for industry [3]) will be maintained rather than the current extreme fidelity imbalances between CFD and CSM used for rotorcraft [15]. For example, under current practices, CFD solutions using millions of grid points are coupled with simple 2-D beam models [15].

In this effort, beam finite element structural equations that are adequate to predict the onset of flutter are used. The primary advantage of beam elements is that they allow a reduction in the number of structural equations while maintaining accuracy in predicting responses. In addition, due to the absence of public-domain aeroelastic test data, they facilitate validation with compatible comprehensive codes. Most tools developed for the 2-D beam elements in the modular C++ environment will also be applicable for use with 3-D finite element method (FEM)-based CSD models to be used later in the program.

Presented as Paper 4199 at the AIAA 39th Fluid Dynamics Conference, San Antonio, TX, 22–25 June 2009; received 1 June 2009; revision received 18 January 2010; accepted for publication 1 February 2010.

*Senior Scientist, Applications Branch, Advanced Supercomputing Division; guru.p.guruswamy@nasa.gov, Associate Fellow AIAA.

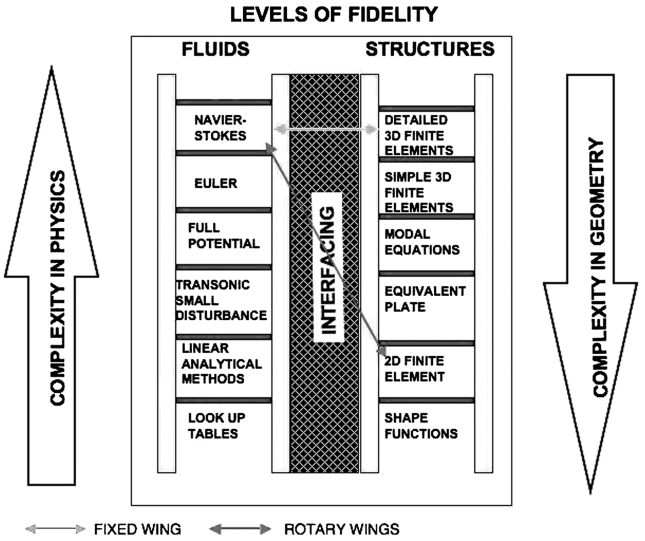

Fig. 1 Levels of fidelity used in fluid–structure interaction computations.

Approach

Domain-Based Approach

When simulating aeroelasticity with coupled procedures, it is common to deal with fluid equations in the Eulerian reference system and structural equations in the Lagrangian system. The structural system is physically much stiffer than the fluid system, and numerical matrices associated with structures are orders-of-magnitude stiffer than those associated with fluids. Therefore, it is numerically inefficient (or even impossible) to solve both systems using a single numerical scheme (see the Sub-Structures section in [18]).

Guruswamy and Yang [6] presented a numerical approach to solve this problem for 2-D airfoils by independently modeling fluids using the finite-difference-based transonic small-perturbation equations and structures using finite element equations. The solutions were coupled only at the boundary interfaces between fluids and structures. The coupling of solutions at boundaries can be done either explicitly or implicitly. This domain-based approach allows one to take full advantage of state-of-the-art numerical procedures for individual disciplines. This coupling procedure has been extended to 3-D problems and incorporated in several advanced aeroelastic codes such as XTRAN3S [19], based on the transonic small-perturbation theory. It was also demonstrated that the same method could be extended to model fluids with the Euler/Navier–Stokes equations on moving grids [10–12,20]. The coupled fluid–structure analysis procedure using a domain-based approach is described in the next section.

To facilitate the domain-based approach, it is assumed that CFD and CSD solvers are independent executables. Interfaces from fluids to structures (FTOS) and structures to fluids (STOF) are also considered separate executables. Activation of executables and communication among them are managed by a C++ executive, RUNEXE [21], and data transfers are made through I/O. Figure 2 shows a flow diagram of the process. This approach provides high modularity to the analysis process in addition to the flexibility of using different CFD and CSD codes. More details about C++ based RUNEXE can be found in [21]. Another advantage of using C++ is that it is portable to other frameworks.

During coupled calculations it is important to monitor convergence data when computations are in progress. Therefore, a 2-D plotting capability based on XMGRACE [22], an open-source software module, is included in the process. In addition, it is necessary to save data for high-end graphics visualization. In this process, a capability has been added to save data using the FieldView format [23] at user-specified intervals. As demonstrated in [21], this approach is efficient for coupling nonlinear flows with nonlinear structures required for the rotorcraft system.

RUNEXE differs from HiMAP in several aspects. One difference is that RUNEXE is independent of a data communication protocol, whereas HiMAP is hard-wired for using the message passing interface. Both internal I/O and TCL/Tk-based [21] data communications have been tested in RUNEXE. In addition, unlike HiMAP, RUNEXE can have dynamic graphics interfaces.

CFD Module

In this paper, the Reynolds-averaged Navier–Stokes solver OVERFLOW (based on the diagonal form of the Beam–Warming central-difference algorithm and the algebraic Baldwin–Lomax turbulence model) with modifications to model rotor blades is used for flow solutions [24]. The latest version of the code OVERFLOW2 is extensively validated for steady flows. In this work, validation is carried out for unsteady flows on flexible blades. An interface has been added that exports blade surface pressures to the FTOS module and reads-in a new deformed grid from the STOF module at every time step.

The strong conservative law form of the Navier–Stokes equations is used for accurate modeling of nonlinear flows. The equation for pressures needed for aeroelastic equations [25] can be written as

$$p = (\gamma - 1)[e - 0.5\rho(u^2 + v^2 + w^2)] \tag{1}$$

where γ is the ratio of specific heats; e is enthalpy; ρ is freestream air density; and u, v, and w are velocities nondimensionalized with the freestream speed of air in the x, y, and z directions, respectively. The time variable used in the Navier–Stokes equations to obtain is nondimensionalized by the ratio of freestream airspeed and chord length of the blade.

CSD Module

The 10-degree-of-freedom beam finite element BEMBLD used in this work (shown in Fig. 3) is a modified version of Bernoulli–Euler beam-theory-based FEM software [26]. The nodal degrees of freedom (DOF) u and w represent flapping and chordwise DOF, whereas θ, α, and ψ represent torsional, chordwise, and flapwise rotation DOF, respectively. It is improved by adding the first-order effects of centrifugal rotation [27] and torsion–bending coupling [28]. This element is well validated for nonrotating cases [26]. Figure 4 shows the validation for a rotating blade [29], for which the average structural properties are given in Table 1. The frequency of the first flapping mode compare well with the shake test for rotor speeds up to $\Omega = 650$ rotations per minute (rpm).

Element properties of BEMBLD are assembled into global properties [26] and incorporated in CSD based on Lagrange's equations of motion:

$$[m]\{\ddot{u}\} + [g]\{\dot{u}\} + [k]\{u\} = \{F\} \tag{2}$$

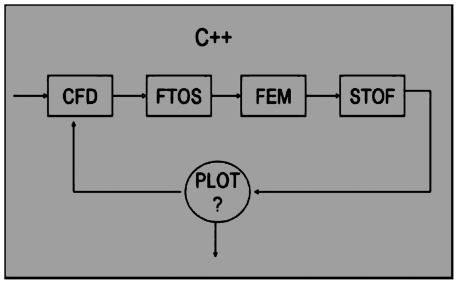

Fig. 2 Flow diagram of analysis process.

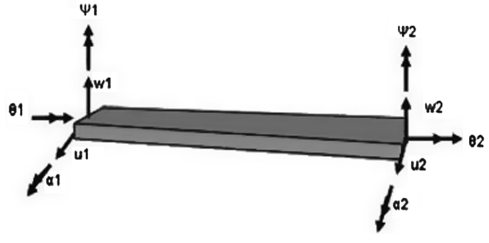

Fig. 3 Ten degree of freedom beam finite element BEMBLD.

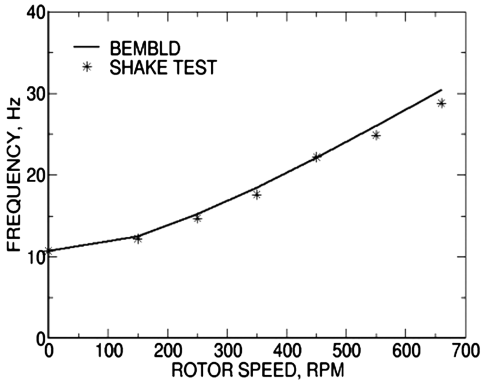

Fig. 4 Effect of rotor speed on the flapping mode frequencies.

where $[m]$, $[g]$, and $[k]$ are mass, damping, and stiffness matrices, respectively. $\{F\}$ is the aerodynamic force vector defined as $1/2\rho U^2\{L\}$, where $\{L\}$ is the aerodynamic global nodal force vector, ρ is the freestream density, and U is the local speed of the blade section.

The aeroelastic equations of motion (2) are solved by a numerical integration method based on the linear-acceleration method [30]. Assuming a linear variation of the acceleration, then velocities and displacements at the end of a time interval $t + \Delta t$ can be derived as follows:

$$\{\dot{u}\}_{t+\Delta t} = \{u\}_t + \left(\frac{\Delta t}{2}\right)\{u\}_t + \left(\frac{\Delta t}{2}\right)\{u\}_{t+\Delta t} \tag{3a}$$

$$\{u\}_{t+\Delta t} = \{u\}_t + (\Delta t)\{\ddot{u}\}_t + \left(\frac{\Delta t^2}{3}\right)\{\ddot{u}\}_t + \left(\frac{\Delta t^2}{6}\right)\{\ddot{u}\}_{t+\Delta t} \tag{3b}$$

$$\{u\}_{t+\Delta t} = [D](\{F\}_{t+\Delta t} - [G]\{v\} - [K]\{w\}) \tag{3c}$$

where

$$[D] = \left([M] + \left(\frac{\Delta t}{2}\right)[G] + \left(\frac{\Delta t^2}{6}\right)[K]\right)^{-1}$$

$$v = \{\dot{u}\}_t + \left(\frac{\Delta t}{2}\right)\{\ddot{u}\}_t$$

$$w = \{u\}_t + (\Delta t)\{\dot{u}\}_t + (\Delta t)\{\ddot{u}\}_t + \left(\frac{\Delta t}{2}\right)\{\ddot{u}\}_t$$

These time integration equations can also be derived by using the second-order time-accurate central-difference scheme, which falls into the explicit form of Newmark's time integration methods [30]. To obtain physically meaningful responses, it is necessary to use the same time step for integration for both the fluids and aeroelastic equations of motion. Though Eqs. (3) are explicit in time, the time-step size required to solve Reynolds-averaged Navier–Stokes equations is an order of magnitude less than that required to solve the aeroelastic equations of motion (3). In addition, the above time integration scheme is nondissipative and does not lead to any nonphysical aeroelastic damping.

Table 1 Structural properties of NASA Langley Research Center blade

Properties	Values
Length L	54.25 in.
Chord c	4.24 in.
Mass per unit length m	0.039 lb/in.
Bending modulus of elasticity E	1.0×10^7 lb/in.^{2}
Torisional modulus of elasticity J	3.7×10^7 lb/in.^{2}
Poisson's ratio ν	0.30
Sectional area A	0.224 in.^{2}
Torsional area moment of inertia J	0.00485 in.^{4}
Flapwise area moment of inertia I_x	0.00151 in.^{4}
Chordwise area moment inertia I_y	0.02447 in.^{4}

The step-by-step integration procedure for obtaining the aeroelastic response is performed as follows. The grid for the flow solver is obtained using a dynamic grid generation module from the ENSAERO code [10], using assumed initial values for displacement $\{q\}$, velocity $\{\dot{q}\}$, and acceleration vectors $\{\ddot{q}\}$. Using this grid, the aerodynamic force vector $\{F\}$ at time $t + \Delta t$ is computed from OVERFLOW2. Based on this aerodynamic vector, the new displacements at time $t + \Delta t$ are computed by solving Eq. (3). This process is repeated every step to advance the aerodynamic and structural equations of motion forward in time until the required response is obtained.

Results

Computations are made for isolated nonrotating and rotating blades. A C-H grid topology with 151 points in the chordwise direction, 45 grid points in the spanwise direction, and 50 points in the normal direction is used.

Nonrotating Blades

Flow computations are made using the OVERFLOW2 code along with the Baldwin–Lomax turbulence model [24]. Accurate prediction of unsteady pressures is a necessary part of aeroelastic computations, and the current unsteady results are validated with well-documented experimental results reported in [31] for a nonrotating blade. In the experiment, a blade with an aspect ratio of 6 and a 6% circular arc section is subjected to forced sinusoidal elastic bending motion, and corresponding unsteady pressure data is measured. Experimental data include steady-state measurements when the blade is not oscillating.

First, steady-state computations for a nonoscillating case are made to check the adequacy of the grid used. Good comparison between computed and measured steady-state data in Fig. 5 demonstrates that the C-H grid size selected is adequate for resolving the transonic flows.

Figure 6 shows the comparison of unsteady pressure between OVERFLOW2 and experiments [31] for $M_\infty = 0.90$ at a reduced frequency $k = 0.26$ based on the chord when the blade is undergoing forced sinusoidal elastic bending motion. Both the magnitude and phase angles of unsteady pressures peak near the shock wave, which are accurately predicted by OVERFLOW2 with 1200 time steps per cycle. It is noted that the linear aerodynamics theory used in the comprehensive code cannot predict unsteady pressure jumps and phase angles associated with moving shock waves. Flapping motions play an important role in the aeroelasticity of rotorcraft.

A nonrotating blade for which a measured pitch-flap flutter boundary is given in [32] is selected to validate the C++ executive RUNEXE. Figure 7 shows the first bending and torsional mode shapes and frequencies computed from BEMBLD. Figure 8 shows the stable, unstable, and neutrally stable responses of the elastic blade.

These responses were computed using a nondimensional time step of 0.01, based on accuracy limits of the flow solver, which is 150 times smaller than the smallest time step required to resolve the first bending mode. This justifies the use of explicit time integration

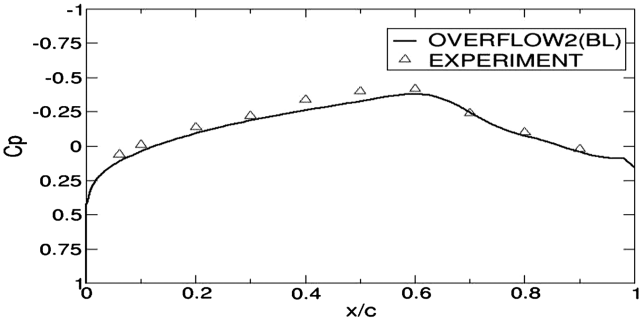

Fig. 5 Comparison of steady pressures at $M_\infty = 0.90$, $\alpha = 0.0$ deg, and $Re = 4.5 \times 10^6$.

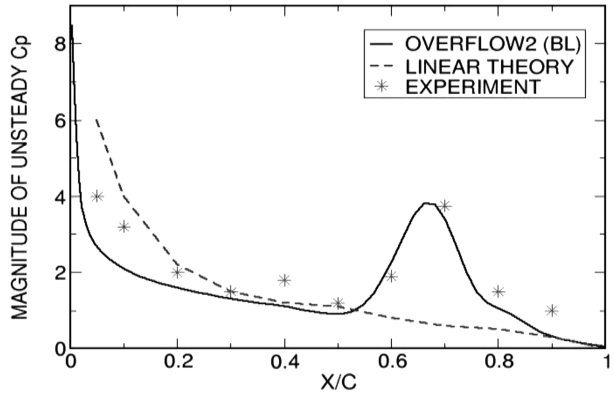

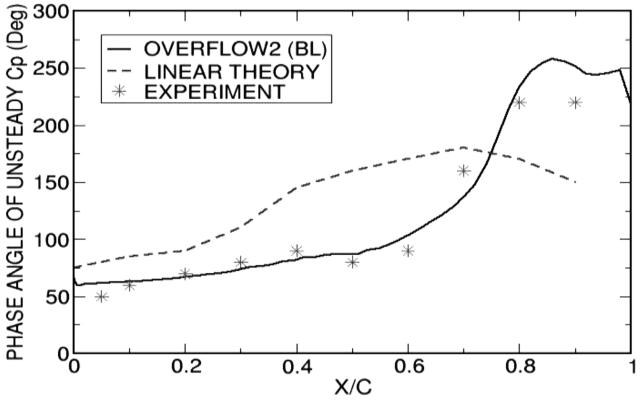

Fig. 6 Unsteady pressures for flapping motion at $M_\infty = 0.90$ and $k = 0.26$.

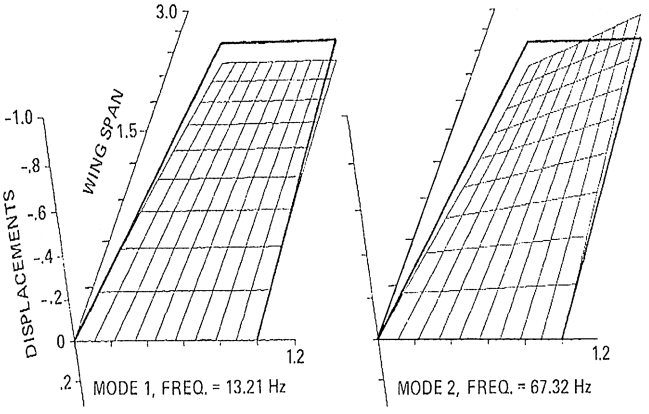

Fig. 7 First two modes of the blade; mode 1 is bending and mode 2 is torsion.

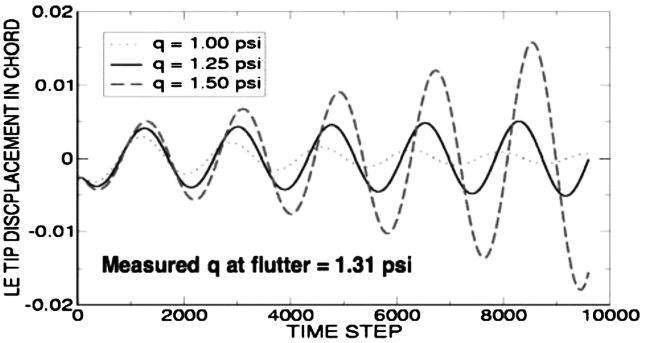

Fig. 8 Dynamic aeroelastic responses at $M = 0.715$ corresponding to measured flutter dynamic pressure $q = 1.31$ psi, from [32].

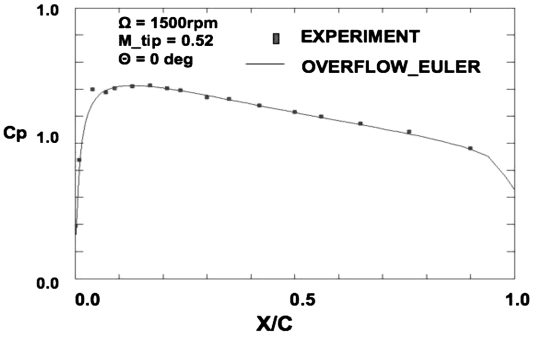

Fig. 9 Comparison of upper surface pressure coefficients for rotating blade.

selected in this work. Dynamic pressure at the neutrally stable condition for Mach 0.715 agrees well with the experiment [32].

Rigid Rotating Blade

Results in Figs. 5–8 establish that aeroelastic computations are accurate when running coupled computations for nonrotating blades. Next, results are demonstrated for a rotating blade, which has an aspect ratio of 6 and a NACA0012 airfoil section [33]. Figure 9 shows the upper surface pressures at the 60% span station when the blade is rotating at 1500 rpm with a zero collective angle of attack in hover. Computed surface pressures converged to a steady state after three rotations and compare well with the experiment.

Figure 10 shows comparison of Euler and Navier–Stokes-equations-based sectional lift coefficients with measured data for the same blade at 1250 rpm with a collective angle of attack of 8 deg. Results from the Navier–Stokes equations compare better than those from the Euler equations beyond 70% span. Results from the lifting-line theory [33] are closer to the Euler solutions beyond 60% span but deviate away as the span station gets closer to the root. Both computed results are within the uncertainty bound stated in the report on experiment [33] for span stations beyond the 60% station.

Flexible Rotating Blade

Aeroelasticity of rotating blades is not as well understood as that of fixed wings. Quite often, it does not appear explicitly, since it is embedded in stability computations and implicitly controlled by trim. With fixed wings, aeroelastic phenomena occur due to the exchange of energy between fluids and structures [34], and phase angles between structural motions and aerodynamic responses play a key role in aeroelasticity [35]. Most studies in aeroelasticity using compressive codes are combined with trim conditions selected based on wind-tunnel data criteria [36]. Independent study of aeroelasticity is required for more complex modern rotor blade configurations.

Nonlinear effects of the flow also play a significant role in rotating wing aeroelasticity, particularly when tip Mach numbers reach the transonic range. As shown in experiments [31], the phase angle takes a jump near the shock wave, which can further impact aeroelastic behavior.

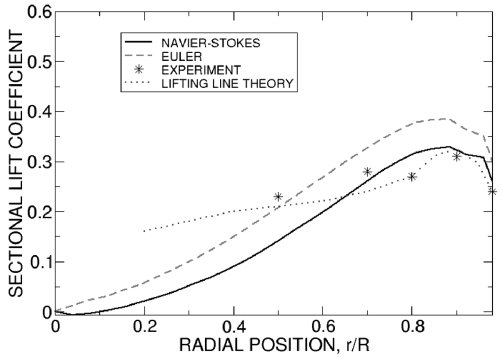

Fig. 10 Comparison of sectional lift coefficient at 1250 rpm and 8 deg collective angle of attack.

Table 2 Structural properties of Massachusetts Institute of Technology blade

Properties	Values
Length L	5.5 m
Chord c	0.65 m
Mass per unit length m	18 kg/m
Axial rigidity EA	1.0×10^8 N
Torsional rigidity GJ	1.0×10^8 N · m^2
Bending rigidity about x axis EI_x	1.1×10^5 N · m^2
Bending rigidity about y axis EI_y	1.0×10^7 N · m^2

Limited aeroelastic experiments are conducted for rotor blades due to added complexities arising from rotations and hub rigid-body motions compared to those of fixed wings. In this paper, a computational model analyzed using a validated linear aerodynamic method [37] is considered for validation. The structural properties of the blade are given in Table 2. The aeroelastic results that do not include the effects of inertial forces are validated for the static model.

The blade is modeled using 10 BEMBLD elements that resulted in 50 nodal degrees of freedom. Figure 11 shows the response of tip displacement with respect to time step at a rotor speed of 15 rad/s. Results are numerically stable for computations made using 2000 steps. The blade was ramped up to a collective pitch angle of 10 deg in 2000 steps. It is noted that for a lower number of steps per revolution, the results numerically diverged after the ramp motion ended. A total of 6000 steps (i.e., three revolutions) were used, at which time the results converged to a static equilibrium state.

Static aeroelastic responses were computed up to a rotor speed of 40 rad/s. Figure 12 shows the favorable comparison between linear aerodynamic computations and present computations. Beyond 30 rad/s, at which the tip Mach number reaches 0.60, the results begin to differ. For Mach numbers above 0.6, linear aerodynamic method possibly becomes less effective. Though one might assume that CFD-based methods are valid at higher Mach numbers, further experimental data are required to confirm results.

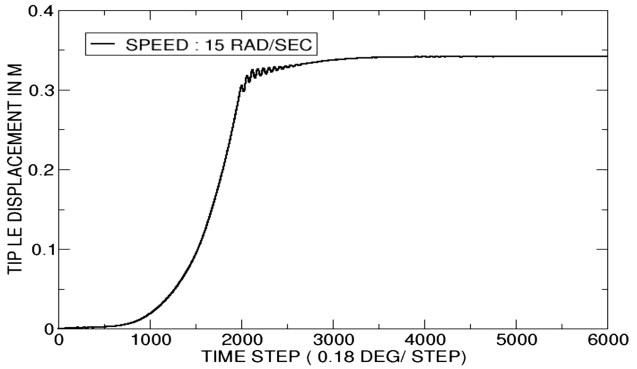

Fig. 11 Aeroelastic response at rotor speed of 15 rad/s.

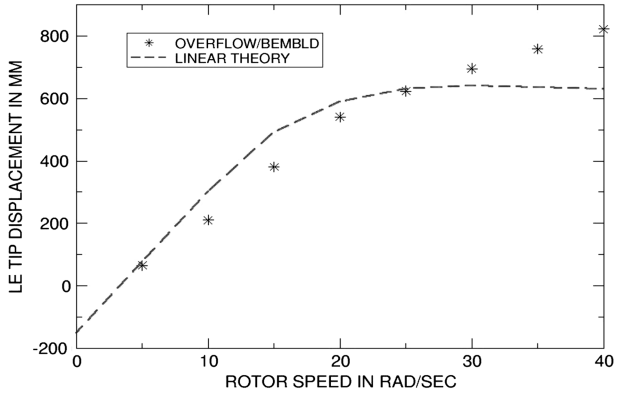

Fig. 12 Comparison of static aeroelastic responses between linear theory and RUNEXE.

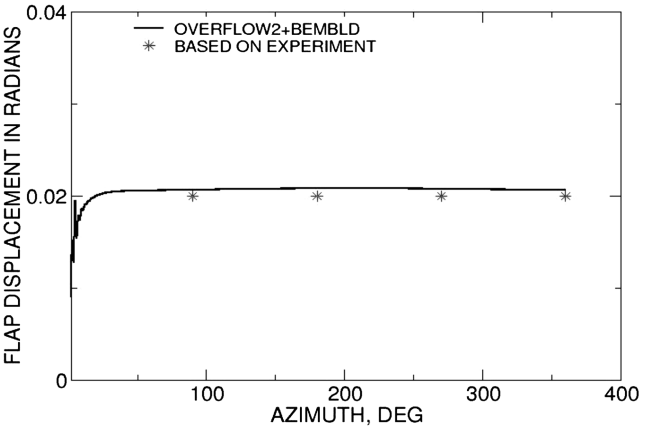

Fig. 13 Comparison of dynamic aeroelastic displacements between RUNEXE and experiment in hover.

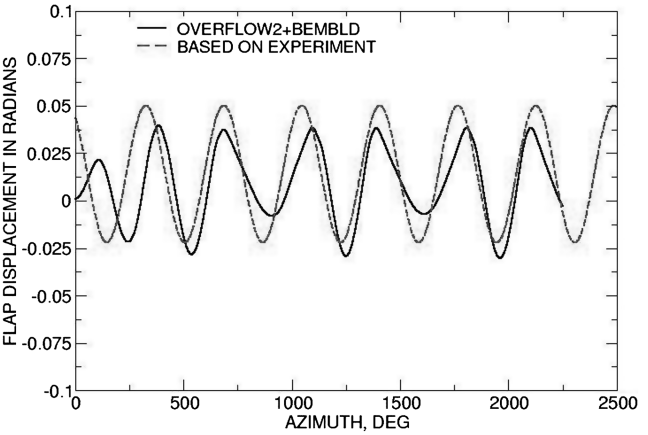

Fig. 14 Comparison of dynamic responses at a rotating speed of 100 rad/s and advance ratio of 0.40.

Dynamic Aeroelastic Computations

Dynamic aeroelastic computations are made for a blade that was tested in a wind tunnel for hover and cruise conditions [38]. The blade was tested for various root conditions with and without gust loads. The blade has an aspect ratio of 15 with NACA0012 airfoil section. In this paper, a case without gust loads in which the response was predominantly in flapping motion with high torsional rigidity is selected. For this case, the blade responded like a rigid blade by only undergoing flapping motion. In the experiment, the collective and cyclic flap deflections as root rotations were measured.

Computations were made using the Euler equations at a rotating speed of 100 rad/s, leading to a tip Mach number of 0.25. Figure 13 shows the good comparison of flap deflection response with the experiment in hover. Time-accurate coupled computations required 0.025 deg of azimuth angle per step in order to obtain stable and accurate results. Computed results converge to steady state within the first quadrant of the motion. The experimental results are based on the collective flap deflection. Because of steady-state hover motion, cyclic flap deflections are not present.

Figure 14 shows the comparison of flap deflection for a cruise condition of 0.40 advance ratio when the blade is rotating at 100 radians per second with a shaft angle of 10 deg. Computations required 14400 steps per rotation and reached harmonic conditions in the second cycle. The computed results compare well both in magnitude and phase with the experimental result which is based on measured collective and the first harmonic cyclic flap deflections.

Conclusions

This work shows that it is practical to time-accurately couple the Euler/Navier–Stokes flow solver with a beam-finite-element-based

structure solver as opposed to the current limited non-time-accurate loosely coupled approaches. The C++ programming language is found to be effective in seamlessly integrating flow and structure solvers by providing a modular and portable computational environment extendable for use with 3-D FEM. The solution procedure presented allows for large movements of flexible components needed to model helicopter blade aeroelasticity. The good comparison of unsteady results with experiments for flexible nonrotating and rigid rotating blades prove the time accuracy of the procedure presented. It resulted in the time-accurate prediction of aeroelastic responses of a nonrotating blade. The procedure demonstrates accurate computation of static aeroelastic responses of a rotating blade up to a rotor speed of 30 rad/s. Dynamic aeroelastic results compare well both in magnitude and phase angles of displacement responses with those results based on wind-tunnel measured data, showing that the present time-accurate coupling procedure is valid.

Acknowledgments

This work was done under sponsorship of the Subsonic Rotary Wing project, a part of the NASA Aeronautics Research Mission Directorate's Fundamental Aeronautics Program.

References

[1] "RCAS Theory Manual, Version 2.0," U.S. Army Aviation and Missile Command, TR 02-A-005, Moffett Field, CA, June 2000.

[2] Johnson, W., "Recent Developments in Rotary Wing Aerodynamic Theory," *AIAA Journal*, Vol. 24, No. 8, 1986, pp. 1219–1244. doi:10.2514/3.9425

[3] Das, M., Madenci, E., and Straub, F. K., "Aeroelastic Analysis of Rotor Blades Using Three Dimensional Flexible Multi-body Dynamic Analysis," AIAA Paper 2007-2295, April 2007.

[4] Bousman, W. G., "Putting the Aero Back in to Aeroelasticity," *Eighth ARO Workshop on Aeroelasticity of Rotorcraft Systems*, Aerospace Engineering Dept., Pennsylvania State Univ., University Park, PA, Oct. 1999.

[5] Ballhaus, W. F., and Bridgeman, J. O., "Numerical Solution Techniques for Unsteady Transonic Problems," AGARD Rept. 679, Neuilly-sur-Seine, France, 1980, pp. 16-1–16-24.

[6] Guruswamy, P., and Yang, T. Y., "Aeroelastic Time Response of Thin Airfoils by Transonic Code LTRAN2," *Computers and Fluids*, Vol. 9, No. 4, 1981, pp. 409–425. doi:10.1016/0045-7930(81)90012-8

[7] McCroskey, J., and Bader, J., "Some Recent Advances in Computational Aerodynamics for Helicopter Applications," NASA TM-86777, Oct. 1985.

[8] Friedman, P., and Hodges, D. H., "Rotary Wing Aeroelasticity—An Historical Perspective," *Journal of Aircraft*, Vol. 40, No. 6, 2003, pp. 1019–1046. doi:10.2514/2.7216

[9] Chopra, I., "Perspective in Aeromechanical Stability of Helicopter Rotors," *Vertica*, Vol. 14, No 4, 1990, pp. 457–508.

[10] Guruswamy, G. P., "Unsteady Aerodynamic and Aeroelastic Calculations for Wings Using Euler Equations," *AIAA Journal*, Vol. 28, No. 3, March 1990, pp. 461–469. doi:10.2514/3.10415; (also AIAA Paper 88-2281, April 88).

[11] Potsdam, M. A., and Guruswamy, G. P., "A Parallel Multiblock Mesh Movement Scheme for Complex Aeroelastic Applications," AIAA Paper 2001-0716, Jan. 2001.

[12] Guruswamy, G. P., "Development and Applications of a Large Scale Fluids/Structures Simulation Process on Clusters," *Computers and Fluids*, Vol. 36, No. 3, 2007, pp. 530–539. doi:10.1016/j.compfluid.2006.03.005

[13] Kunz, D. L., "Comprehensive Rotorcraft Analysis: Past, Present and Future," AIAA Paper 2005-2244, April 2005.

[14] Potsdam, M., Yeo, H., and Johnson, W., "Rotor Airloads Prediction Using Loose Aerodynamic/Structural Coupling," *AHS 60th Annual Forum* [CD-ROM], AHS International, Alexandria, VA, June 2004.

[15] Nygaard, T. A., Saberi, H., Ormiston, R. A., Strawn, R. C., and Potsdam, M., "CFD and CSM Coupling Algorithm and Fluid Structure Interface for Rotorcraft Aeromechanics in Steady and Transients Flight Conditions," *AHS 62nd Annual Forum* [CD-ROM], AHS International, Alexandria, VA, May 2006.

[16] Bhagwat, M. J., Ormiston, R. A., Saberi, H. A., and Xin, H., "Application of CFD/CSD Coupling for Analysis of Rotorcraft Airloads and Blade Loads in Maneuvering Flight," *AHS 63rd Annual Forum*, *AHS 62nd Annual Forum* [CD-ROM], Alexandria, VA, May 2007.

[17] Dimanlig, A., Meadowcroft, and Strawn, R., "Modeling of the CH-47 Helicopter in Hover," *AHS 63rd Annual Forum*, *AHS 62nd Annual Forum* [CD-ROM], Alexandria, VA, May 2007.

[18] Zienkiewicz, O. C., Taylor, R. L., and Zhu, J. Z., "Substructures," *The Finite Element Method: Its Basis and Fundamentals*, 3rd ed., McGraw–Hill, New York, 1977, pp. 132–134.

[19] Borland, C. J., and Rizzetta, D., "XTRAN3S-Transonic Steady and Unsteady Aerodynamics for Aeroelastic Applications, Vol. I—Theoretical Manual," Air Force Wright Aeronautical Labs., TR-80-3107, Dayton, OH, Dec. 1985.

[20] Guruswamy, G. P., "ENSAERO—A Multidisciplinary Program for Fluid/Structural Interaction Studies of Aerospace Vehicles," *Computing Systems in Engineering*, Vol. 1, Nos. 2–4, 1990, pp. 237–256. doi:10.1016/0956-0521(90)90011-9

[21] Guruswamy, G. P., "A New Modular Approach for Tightly Coupled Fluid/Structure Analysis," *International Journal of Aerospace Innovations*, Vol. 1, No. 1, March 2009, pp. 1–10.

[22] XMGRACE, Software Package, Ver. 5.1.22, Free Software Foundation, Inc., Cambridge, MA, 2008.

[23] Fieldview, Software Package, Ver. 6, Intelligent Light, Lyndhurst, NJ, May 1999.

[24] Meakin, R., "Unsteady Simulation of the Viscous Flow About a V-22 Rotor and Wing in Hover," AIAA Atmospheric Flight Mechanics Conference, AIAA Paper 95-3463-CP, Baltimore, MD, Aug. 1995.

[25] Peyret, R., and Viviand, H., "Computation of Viscous Compressible Flows Based on Navier–Stokes Equations," AGARD AG-212, Neuilly-sur-Seine, France, 1975.

[26] Guruswamy, G. P., "Special Purpose Finite Element Programs," *Finite Element Structural Analysis*, edited by T. Y. Yang, Prentice–Hall, Upper Saddle River, NJ, 1986, pp. 481–535.

[27] Hurty, W. C., and Rubinstein, M. F., "Vibration of Rotating Beam," *Dynamics of Structures* Prentice–Hall, New Delhi, India, 1967, pp. 182–184.

[28] Banerjee, J. R., "Coupled Bending-Torsional Dynamic Stiffness Matrix of Beam Elements," *International Journal for Numerical Methods in Engineering*, Vol. 28, No. 6, 1985, pp. 1283–1298. doi:10.1002/nme.1620280605

[29] Wilkie, W. K., Mirick, P. H., and Langston, C. W., "Rotating Shake Test and Modal Analysis of Model Helicopter Rotor Blade," NASA TM 4760, June 1997.

[30] Bathe, K. J., "Direct Integration Methods," *Finite Element Procedures*, Prentice–Hall, Upper Saddle River, NJ, 2001, pp. 769–784.

[31] Lessing, H. C., Troutman, J. L., and Menees, G. P., "Experimental Determination of the Pressure Distribution on a Rectangular Wing Oscillating in the First Bending Mode for Mach Numbers 0.24 to 1.30," NASA TN D-344, Dec. 1960.

[32] Dogget, R. V., Rainey, A. G., and Morgan, H. G., "An Experimental Investigation on Transonic Flutter Characteristics," NASA TMX-79, Nov. 1959.

[33] Caradona, F. X., and Tung, C., "Experimental and Analytical Studies of a Model Helicopter Rotor in Hover," NASA TM 81232, Sept. 1981.

[34] Fung, Y. C., "Flutter Phenomenon," *Introduction to the Theory of Aeroelasticity*, Dover, New York, 1955, pp. 163–185.

[35] Guruswamy, P., "Aeroelastic Stability and Time Response Analysis of Conventional and Super Critical Airfoils in Transonic flow by Time Integration Method," Ph.D. Thesis, Purdue Univ., Purdue, IN, 1980.

[36] Lim, J. W., Tung, C., and Hu, Y. H., "Prediction of Blade-Vortex Interaction Airloads with Higher-Harmonic Pitch Controls Using the 2GCHAS Comprehensive Code," *Journal of Pressure Vessel Technology*, Vol. 123, Nov. 2001, pp. 469–474. doi:10.1115/1.1401025

[37] Minguet, P., and Dugundji, J. B., "Experiments and Analysis for Composite Blades Under Large Deflections, Part 1: Static Behavior," *AIAA Journal*, Vol. 28, No. 9, 1990, pp. 1573–1579. doi:10.2514/3.25255

[38] Yasue, M., "Gust Response and Its Alleviation for Hinge less Helicopter Rotor Blade in Cruising Flight," Ph.D. Thesis, Dept of Aeronautics and Astronautics, Massachusetts Inst. of Technology, Cambridge, MA, Aug. 1977.